Additive Manufacturing 27 (2019) 363–371

Contents lists available at ScienceDirect

Additive Manufacturing

journal homepage: www.elsevier.com/locate/addma

Review of acrylonitrile butadiene styrene in fused filament fabrication: A plastics engineering-focused perspective

Amy M. Peterson

University of Massachusetts Lowell, Department of Plastics Engineering, Lowell, MA, United States

ARTICLE INFO

Keywords:
ABS
Fused filament fabrication
Material extrusion additive manufacturing

ABSTRACT

To date, the materials used for fused filament fabrication (FFF) are commercially available plastics that can be extruded, such as acrylonitrile butadiene styrene and poly(lactic acid). Many other polymers are available in filament form, including polycarbonate, polycaprolactone, polyetherimide, poly(ether ether ketone), and poly (ether ketone ketone). Although each of these materials is commonly referred to by its polymer structure and thought of as a single material, filaments have unique formulations that include small molecule plasticizers and pigments, as well as different polymer molecular weights and distributions. All of these variations can result in differences in optimal processing windows and performance of the final printed structure. This review provides an introduction to plastics engineering, and places the literature on processing-structure-property relationships in FFF within the context of plastics engineering. From this perspective, the review discusses and attempts to explain some of the conflicting reports relating print parameters and mechanical performance throughout the literature. The review will also include recommendations for filament characterization methods.

1. Introduction

Additive manufacturing (AM) is an increasingly important aspect of modern manufacturing. AM offers the potential for preparation of complex structures that could not previously be achieved, or which could only be achieved with significant waste. One form of polymer AM is material extrusion additive manufacturing (MatEx), in which a material is extruded layer-by-layer onto a print bed. The bed can be heated and the material (polymer, polymer composite, complex fluid, etc.) is deposited through a nozzle. Depending on the nature of the print material, there may be an extruder that heats the material such that it can flow prior to deposition, or a pressure may be applied for shear thinning fluids. Although MatEx structures tend to have inferior mechanical properties, it is widely used due to its versatility and scalability.

Focusing on thermal MatEx, extrusion-based AM ranges from fused filament fabrication (FFF), the most common form of polymer AM with nozzle diameters < 1 mm, up to big area additive manufacturing (BAAM), a large-scale form of MatEx with nozzle diameters 5–10 mm that is capable of printing cars, wind turbine blade tooling, and other large scale structures. In all forms of thermal MatEx, a thermoplastic is extruded through a rastering nozzle onto a print bed as structures are assembled layer-by-layer. The extrudate cools rapidly as a weld forms between the lower layer and the extrudate. Extruders in an FFF context (also referred to as liquefiers) heat a filament to in order to create a polymer melt, which is then pushed through a nozzle in order to form the extrudate bead.

Many FFF processing parameters can be controlled and may affect the properties of the printed part. Parameters include print speed (v_{print}), extruder temperature (T_{ext}), print bed temperature (T_{bed}), print orientation raster orientation, layer thickness, and filament and nozzle diameter [1–13]. From a production perspective, the goal is to achieve the necessary physical and mechanical property-based specifications while minimizing print time and material used. While there has been substantial investigation of FFF, including modeling approaches to address some aspects of achieving this goal, no fundamental science- and engineering-based approach to this broad challenge currently exists [2,14–18]. Therefore, significant amounts of trial-and-error and/or operator experience are currently required to print new structures.

To date, the materials used for FFF are commercially available plastics that can be extruded. FFF commonly uses acrylonitrile butadiene styrene (ABS) and poly(lactic acid) (PLA) [19–22]. Many other polymers are available in filament form, including polycarbonate (PC), polycaprolactone (PCL), polyamides, polyetherimide (PEI), poly(ether ether ketone) (PEEK), and poly(ether ketone ketone) (PEKK). Although each of these materials is commonly referred to by its polymer structure and thought of as a single material, filaments have unique formulations that include small molecule plasticizers and pigments, as well as different polymer molecular weights and distributions. All of these

E-mail address: amy_peterson@uml.edu.

https://doi.org/10.1016/j.addma.2019.03.030
Received 10 January 2019; Received in revised form 21 March 2019; Accepted 26 March 2019
Available online 27 March 2019

variations can result in differences in optimal processing windows, offgassing during printing, and performance of the final printed structure.

This review provides an introduction to plastics formulation, how these modifications can affect printing and performance, and places the literature on processing-structure-property relationships in FFF within the context of plastics engineering. Since ABS is by far the most commonly printed material, it is the focus of this review of processing-structure-property relationships in FFF, and mechanical properties of printed ABS structures reported in the literature over the past 15+ years are summarized. This review also includes recommendations for filament characterization methods.

2. Plastics formulation and filament fabrication

Although the terms plastic and polymer are often used interchangeably, they have distinct meanings. A polymer is a macromolecule consisting primarily of repeating units with sufficient size that the addition of a small number of repeat units does not affect its physical properties. (However, substantial increases in molecular weight will affect viscosity and mechanical properties.) A plastic is an engineered material that consists primarily of one or more polymers, but also contains additives that improve processability, performance, appearance, and/or cost. These additives tend to be smaller molecules and can include plasticizers, pigments, reinforcements, antioxidants, and flame-retardants.

ABS, the most common FFF material, is a general term used to describe many blends and copolymers of acrylonitrile-, butadiene-, and styrene-containing polymers. ABS was introduced in the 1950's as a tougher alternative to styrene-acrylonitrile (SAN) copolymers. At that time, ABS systems were blends of SAN and acrylonitrile-butadiene copolymers, more commonly known as nitrile rubber [23]. Polybutadiene is not chemically compatible with the SAN chains, so the system phase separates, resulting in a dispersed nitrile rubber phase within a continuous SAN phase. Since nitrile is rubbery at room temperature and SAN is glassy, this structure results in an amorphous, glassy, tough, impact resistant material.

Today, ABS typically refers to a system of SAN and lightly cross-linked polybutadiene (rubber) particles that are grafted with SAN to improve dispersion. ABS system variables include the ratios of SAN:polybutadiene in the blend and styrene:acrylonitrine in the SAN; amount of grafted SAN; rubber particle size and size distribution; and rubber cross-link density [23]. ABS formulations often include additives to improve flow during processing, pigments to add color, and anti-oxidants/UV absorbers to prevent degradation and maintain vibrant colors. Although ABS is the most commonly printed material and the bulk of the FFF literature uses ABS, the complex morphology, range of compositions, and effects of additives make ABS a poor model system. However, other candidate materials have a range of other significant drawbacks.

Plastics used in FFF and reported in the literature are summarized in Table 1. After ABS, PLA is the most commonly printed plastic. While PLA is polymerized from a single monomer, its use as a model material is complicated by the fact that PLA is a semi-crystalline polymer. PCs represent a family of polymers that contain a carbonate moiety and a bisphenol A moiety. PCs are amorphous, which is desirable in a model FFF material. However, exposure to water results in embrittlement and significant difficulty in printing when pure PC polymer, instead of engineered plastic PC is used. Other plastics in the FFF literature tend to be high temperature, high cost, and/or are highly modified plastics formulations.

Processing dictates polymer conformation and, therefore, polymer properties. Additionally, plastic formulations are designed to facilitate processing. Common plastics processing methods include injection molding, extrusion, compression molding, thermoforming, blow molding, and rotational molding. For the purposes of this review, we will focus on injection molding and extrusion – injection molding because it is the most common method of polymer processing/most likely competitor for FFF structures and extrusion because 1) it is the next most common method of processing, with distinct advantages and challenges as compared to injection molding; 2) filaments for FFF are extruded; 3) FFF is also an extrusion process.

In injection molding, parts are fabricated through injecting a shot of molten plastic into a mold. Molds can be quite complex, which allows for incorporation of product design features that would otherwise require additional processing. However, injection molding is not appropriate for highly loaded composites, or for long fiber composites. While injection molding requires substantial investments of time and money for tooling fabrication, it is capable of rapid production and fabrication of multiple parts simultaneously. In injection molding, plastic pellets are fed to a process. In order to induce flow, energy is added to the pelletized plastic to create a "melt" – it is important to note that the melt describes a material that flows, and not necessarily a material that is above its melt temperature, as this terminology also applies to amorphous polymers. The melt is injected into the mold under high temperature and pressure, then the injection molded part is cooled. The part must be cool enough to not flow/warp once the mold is opened, which is challenging because polymers are thermal insulators [76].

In extrusion, products are designed as a 2D cross-section that is extruded in the third dimension, which limits the possible part geometries to structures like sheets and films, cylindrical or tubular fibers, and pipes. However, extrusion is a continuous process, which allows for higher production rates [76]. Die swell, or extrudate swell, and orientation are important design considerations for extrusion. Die swell describes when an extrudate swells to a size greater than the die from which it came due to polymer entanglement as well as the drop in pressure upon extrusion. Orientation refers to polymer chain alignment, and occurs as a result of flow in a single direction. Orientation may be desirable because it can improve the properties of the product. Orientation also allows an extruded product, like shrink wrap, to shrink when exposed to heat. Similar behavior has been observed in FFF structures [4,77].

3. Polymer weld theory and its application to FFF

Since temperature changes in FFF are rapid and determine polymer behavior including interlayer diffusion and residual stresses, thermal profiles have been investigated experimentally and via simulation. Temperatures have been measured in FFF by infrared (IR) thermography or with thermocouples. MatEx structures rapidly cool, with a newly extruded road of ABS cooling below its glass transition temperature (T_g) within seconds [7,78–80]. Experimental temperature measurements are limited in location (to a single point for thermocouples or on/near the surface for IR thermography). *in situ* measurement limitations can be addressed with *in silico* approaches. Thermal simulation measurements have ranged from 1D simulations along the length of a deposited filament [2,81] to 2D simulations normal to the road axis [82] to full 3D heat transfer models [15–18,83–87].

While temperature and shear history are important to the behavior of all polymer systems, different types respond in different ways. Amorphous polymers, such as ABS and PC, will exhibit molecular weight dependence [88–90]. They may also exhibit strain-induced segregation, with specific phases preferentially orienting towards the exterior or center of the extruded road [91,92]. In semi-crystalline polymers, such as PLA and PCL, the role of temperature- and shear rate-dependent crystallization also becomes a concern [93–96]. Composites add additional complexity, with clear compositional heterogeneity on the size scale of the reinforcing phase. Additionally, reinforcement orientation can lead to property anisotropy, while reinforcement-polymer adhesion affects composition of the melt phase and stress transfer in the final part [97–99].

In FFF, the extrudate is a flowing polymer experiencing a large shear

Table 1
Summary of non-ABS plastics printed using FFF. HIPS = high impact polystyrene, LDPE = low density polyethylene, PE = polyethylene, PET = poly(ethylene terephthalate), PETG = polyethylene terephthalate glycol, PP = polypropylene, PPS = poly(phenylene sulfide), TPU = thermoplastic polyurethane, PVP = poly(*N*-vinylpyrrolidone), PVAL = poly(vinyl alcohol), SEBS = styrene-ethylene/butylene styrene, UHMWPE = ultra-high molecular weight polyethylene.

Polymer	Ref.
HIPS	[24,25]
Hydroxypropyl-methylcellulose	[26]
LDPE	[27]
PC	[25,28,29,30,31]
PCL	[32,33]
PE wax	[34]
PEEK	[8,20,35,36,37,38,39]
PEI (including Ultem)	[9,40,41]
PET	[42]
PETG	[25]
PLA	[33,43,44,45,46,47,48,49,50,51,52,53,54,55,56,57,58,59,60,61,62,63,64]
Polyamide (including Nylon)	[25,65,66,67]
Polydioxanone	[33]
Polyester	[65]
Polyglycolide	[33]
Polythiourethane	[68]
PP	[30,69]
PPS	[37]
TPU	[1,61]
PVP-PVAL copolymer	[70,71,72]
ABS/SEBS blend	[73]
ABS/UHMWPE/SEBS blend	[73,74]
PC/ABS blend	[75]
PEI/PC blend	[41]
PEI/PETG blend	[41]

gradient as it passes through the nozzle that then undergoes a 90° re-orientation upon deposition. McIlroy and Olmsted reported non-axisymmetric disentanglement of an extruded amorphous polymer, with significant disentanglement along the outer edge and a gradient of disentanglement and normal stress along the height of the road [91]. The resulting weld would be anisotropic and also relatively disentangled, which would further lower weld strength [88].

One way FFF differs from traditional processing methods is that samples cool rapidly, on the order of 10 K/s. This results in 1) the trapping of polymers in highly non-equilibrium conformations; 2) limited time for polymer diffusion at road interfaces; 3) complex crystallization profiles for semi-crystalline polymers. In Fig. 1, differential scanning calorimetry (DSC) of portion of the top and bottom of a single PLA specimen 30 mm in height is provided, which provides an example of the variation in crystallinity possible across a single FFF structure. The melt peak at ~148 °C from the first DSC heating gives a measure of the amount of crystallinity. In the case of PLA, the enthalpy of cold crystallization (ΔH_c, observed at ~114 °C) must be subtracted from melt enthalpy (ΔH_m) in order to determine percent crystallinity due to processing. Given a heat of fusion (ΔH_f) of 93 J/g [100], the bottom of the sample exhibits 2.9% crystallinity, while the top of the sample exhibits 1.9% crystallinity. The T_g of the bottom is also slightly (57.8 °C vs. 56.6 °C) higher than that of the top.

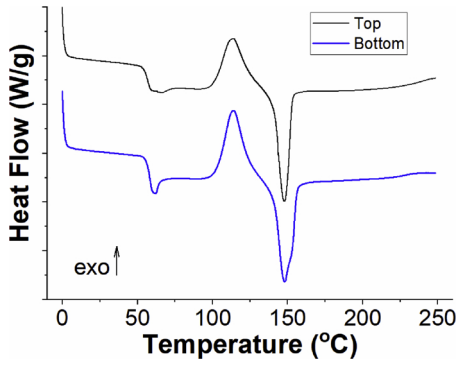

Fig. 1. DSC of two locations in a 30 mm tall PLA FFF structures. First heating, 10 K/min. Curves are shifted vertically to avoid overlapping. Each major y-axis tick represents 0.2 W/g.

Thermal transitions in polymers occur due to different scales of molecular relaxation. The two major transitions in polymers are the glass and melting transitions. The glass transition is associated with local main chain movement and occurs within amorphous regions of a polymer, while the melting transition is associated with chain slippage and occurs with crystalline regions of a polymers. Since these transitions are related to long-range motion, below these thermal transitions, the time scale necessary for flow to occur in corresponding regions of a polymer is considered to be so large that such motion is neglected. Therefore, welding is said to occur at temperatures above the T_g for amorphous polymers or crystallization temperature (T_c) for semi-crystalline polymers.

Time-temperature superposition (TTS) states that phenomena occurring over long time periods at low temperatures are equivalent to phenomena occurring over short time periods at elevated temperatures. TTS is very useful for determining mechanical properties of linear viscoelastic materials at temperatures or times that cannot be reached experimentally. For non-isothermal processes such as FFF, TTS can be a useful principle for normalizing all time-temperature information to equivalent isothermal time at a reference temperature. For amorphous polymers, this relationship can be described using the Williams-Landel-Ferry (WLF) equation:

$$\log a_T = \frac{-C_1(T - T_r)}{C_2 + (T - T_r)}$$

where C_1 and C_2 are material-specific constants determined by fitting to a master curve, a_T is the shift factor, and T_r is the reference temperature [17,101]. This approach has been used to calculate equivalent isothermal weld times for FFF [2,6,17]. In polymer processing, an Arrhenius approach is regularly used in combination with TTS for characterization of semi-crystalline polymers [102].

Interdiffusion between two polymer layers has been investigated thoroughly since the early 1980's in the service of polymer welding

[89,90,103,104]. Renewed interest in this area began in the mid-2000's related to self-healing materials [105–109]. As a result, there is a wealth of knowledge that can be applied to characterizing and understanding polymer interdiffusion between roads in MatEx. Polymer interdiffusion, which derives from random molecular motion of polymer chains, requires that the two surfaces are capable of wetting such that chains motion across the interface is possible. While there are multiple microscopic models that have been proposed to describe the time dependence of properties during welding/healing [89,104,110,111], all lead to the conclusion that fracture energy (G_{IC}) is proportional to $t^{1/2}$ and fracture stress (σ) and stress intensity factor (K_{IC}) are proportional to $t^{1/4}$, where t is the isothermal weld time. This proportionality holds until complete interdiffusion is achieved, at which point bulk mechanical properties are observed.

In order to apply polymer weld theory to MatEx, which is a highly non-isothermal welding process, TTS is used to condense all time-temperature information to a single isothermal weld time. Then, mechanical properties can be plotted as a function of this time t. TTS and polymer weld theory have been shown to be effective approaches to understanding and characterizing FFF performance and resulting structure properties [2,6]. Seppala and colleagues found that the classical polymer weld theory $t^{1/2}$ relationship held across a range of T_{ext} [112]. Two interesting findings of their work: 1. v_{print} does not affect isothermal weld time as substantially as moderate changes in T_{ext}; 2. At very high T_{ext} (270 °C), the $t^{1/2}$ relationship no longer holds, presumably because of some level of polymer degradation along the road exterior.

4. Performance of FFF structures

Since ABS is the most commonly printed material, a review was made of the FFF literature focusing on mechanical performance of ABS structures. Fig. 2 shows reported tensile strengths of FFF-printed ABS since 2002 [4,5,8,11,20,21,25,29,43,66,92,113–136]. These results include all print orientations, so some tensile strengths represent weld (or z-) strength, others report tensile strength normal to the direction of extrusion, and yet others values report tensile strength at orientations in between those two extremes where printed roads are subjected to tensile as well as shear stresses. These results also include many different print parameters, ABS grades, and printers, which will be discussed in greater detail below.

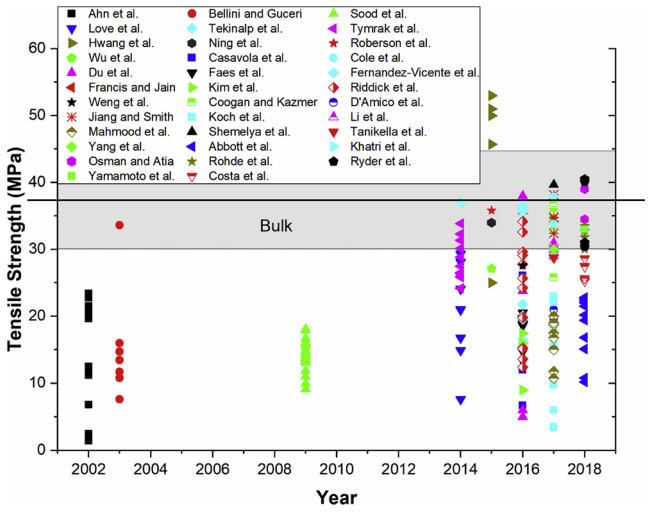

Fig. 2. Tensile strength values for FFF-printed ABS reported in the literature. Each point represents the average of a print condition reported in the literature. The average of bulk tensile strength values reported in the literature and one standard deviation are represented as the solid horizontal line and the gray area on either side of the line, respectively.

The first thing to note about Fig. 2 is the rapid increase in publications since 2014. The first few reports appear in the early 2000's, with generally low tensile strengths. There are no publications that report FFF-printed ABS tensile strength 2004–2008, then one in 2009, and none again until 2014. However, from 2014 on, the number of publications reporting tensile strength of ABS increased to a maximum of 9 each in 2016 and 2017.

It is also interesting to note that substantial improvements in tensile strength have not been achieved since 2014. The maximum values achievable since 2014 have been within one standard deviation of median literature values for bulk ABS [5,8,20,21,66,113,115,118,121,123,125,126], so the lack of continued improvement in performance is likely because we are reaching maximum values. Hwang et al. report the highest tensile strengths in the literature for FFF-printed ABS [116]. This may be due to a combination of material selection and print parameters, but no information about the source of ABS was provided and minimal processing conditions were given in the article, so no firm conclusions can be reached.

To further investigate the hypothesis that we are capable of reaching bulk mechanical properties in ABS structures fabricated with FFF, results from studies that included comparable testing of a traditionally manufactured (bulk) specimen were compiled and are shown in Fig. 3 [5,8,20,21,66,112,113,115,118,121,123,125,126]. While bulk values are achievable for tensile properties, they often cannot be achieved simultaneously. For example, while Fernandez-Vicente et al. report bulk strain to failure, that strain corresponds with < 50% of bulk tensile strength and Young's Modulus. Similarly, for the conditions that achieved 100% of bulk Young's modulus (T_{ext} = 225 °C, T_{bed} = 90 °C, layer thickness = 0.35 mm, 0° raster orientation), Casavola et al. reported 81% of tensile strength. One exception is reported by Tekinalp et al., whom found higher tensile strength than compression molded ABS [115].

Compressive and mode III (tear) testing have also been performed on FFF structures and bulk specimens [20,21,112]. However, there are substantially fewer reports than for tensile testing. Ahn et al. achieved effectively bulk compressive strength of printed ABS for specimens loaded parallel to the build direction (i.e., the cylindrical specimen was printed with the circular cross-section in the z-axis). Wu et al. attributed the low compressive properties of FFF-printed ABS to the "extensive pores" in these structures [20]. Seppala et al. performed mode III fracture experiments on single road width "walls" in order to characterize interlayer strength. Tear energy increases linearly with the square root of isothermal weld time for $T_{ext} \leq 250$ °C, consistent with

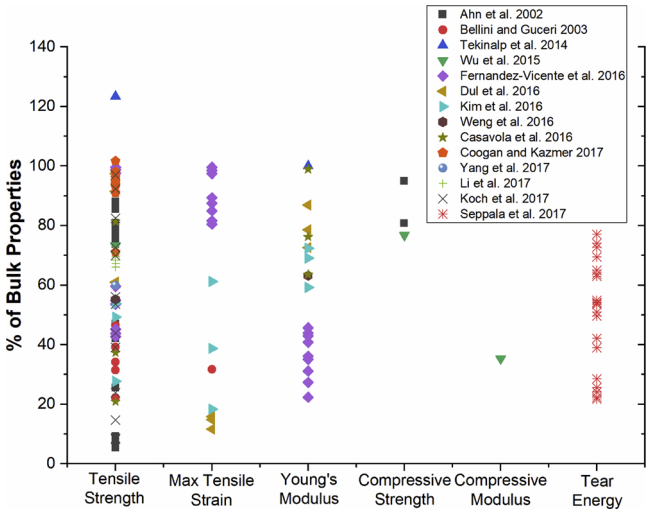

Fig. 3. Mechanical properties of FFF-printed ABS reported in the literature, normalized to reported bulk properties from the same source. Each point represents the average of a print condition reported in the literature.

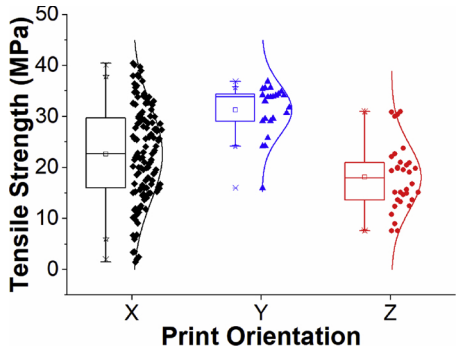

Fig. 4. Literature tensile strengths as a function of print orientation. Data are presented as box plots, scatter plots, and normal distribution curves.

TTS and polymer weld theory as discussed above [112]. Therefore, tear energies from these experiments peak at ~80% of hot pressed ABS sheets due to the limited amount of time available for interlayer diffusion in this geometry for ABS.

The literature results in Fig. 1 include all print orientations. To further explore the idea that a major cause of the wide range of tensile strengths is different print orientations, the data from Fig. 1 was re-plotted according to print orientation and is displayed in Fig. 4. For structures printed in the x and y orientation, failure occurs through a mixture of tensile failure of the roads and shear failure of the welds between roads – the relative amount of each of these failure modes will depend on the raster orientation. Therefore, one would suppose that x- and y-oriented prints would have similar means and distributions of reported tensile strengths. For structures printed in the z orientation, failure occurs primarily through tensile failure of the welds between roads. Since interlayer welds are weaker than the bulk (roads), one would expect that z-oriented prints would exhibit a lower mean tensile strength than x- and y-oriented prints. The population means for each orientation are significantly different at > 99.99% confidence interval ($p = 2.8 \times 10^{-7}$) based on a one-way analysis of variance (ANOVA). The y print orientation has the highest mean with the narrowest distribution – this may result from there being fewer and more recent reports of y-oriented prints as compared to x-oriented prints. Z-oriented prints have the lowest mean tensile strength, which is consistent with the idea that welds are the weakest area in FFF structures. However, x-oriented prints do not exhibit a substantially higher mean and have the broadest distribution of tensile strengths.

Possible sources for the broad distribution of tensile strengths for x-oriented ABS FFF structures include print parameters, ABS grade, and printer. Since the importance of print parameters has been widely reported elsewhere [1–8,11,13], this review will focus on ABS grade and printer. Tensile strengths for x-oriented specimens are presented in Fig. 5 grouped by ABS grade [5,8,11,21,25,66,92,115,120,121,123–125,127,128,130–132,134,135,137] and in Fig. 6 by printer [5,20,21,25,43,92,113–115,118,120,121,123,124,127,128,130,131,133,135,136]. These data only include reports that specified ABS grade (for Fig. 5) or printer (for Fig. 6); therefore, some data in Fig. 4 could not be used.

From Fig. 5, much of the spread in tensile strength might be attributable to a few reports/grades of ABS. P400 was the original grade of ABS used in Stratasys printers, which was replaced by ABS-M30. ABS-M30 has been marketed as a stronger option, and the literature supports that claim. Only one report used MatterHackers ABS, which had the next lowest minimum tensile strength. In it, they investigated the "solidity ratio", or volume fraction of the specimen that consists of ABS. A

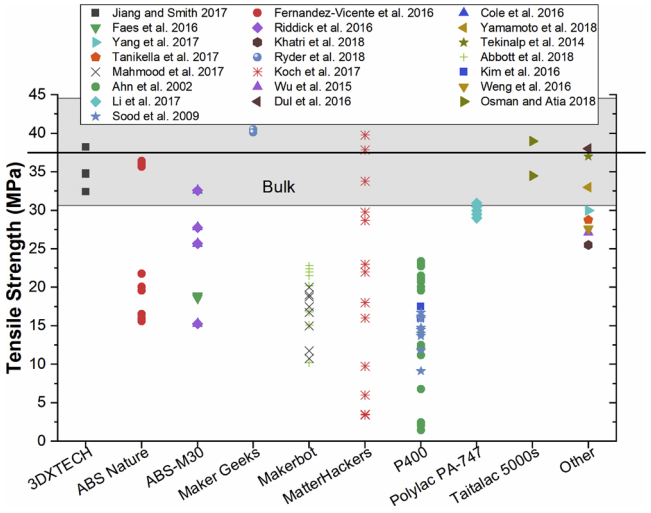

Fig. 5. Literature tensile strengths for x-oriented FFF-printed structures by ABS source. Each point represents the average of a print condition reported in the literature. The average of bulk tensile strength values reported in the literature and one standard deviation are represented as the solid horizontal line and the gray area on either side of the line, respectively.

higher solidity ratio corresponds with a lower void fraction. Tensile strengths less than 20 MPa reported by Koch et al. are for low solidity ratios (< 0.9) [5]. Grade-specific performance of FFF structures was previously investigated by Khaliq et al., who directly compared the rheological characteristics, printability, and mechanical performance of two grades of ABS [138]. They found that the lower viscosity ABS resulted in prints with higher flexural strength.

Table 2 summarizes the print conditions for each of the tensile strengths within one standard deviation of bulk. Near-bulk tensile strengths are reported for T_{ext} = 204–250 °C and v_{print} = 33.3–105 mm/s, which represent most of the printable range for both parameters. These results highlight that different grades of ABS may exhibit unique temperature-dependent rheology that must be considered to achieve a high quality print.

Printer selection was also investigated as a potential source of variation in tensile strength. A summary of the literature is given in Fig. 6. In general, printers and printing ecosystems that provide greater opportunities for customization result in higher tensile strengths. This finding should not be particularly surprising, since customization within a research and development setting allows for iterative improvements.

5. Filament characterization methods

Since filament compositions can vary substantially across a type of plastic in ways that will affect printability and the printed structure's performance, at minimum, the source and color of filament used in all studies should be reported and kept constant across a set of experiments. Filament characterization can also provide useful information for understanding material-processing-structure-property-performance relationships, for comparing results, and for identifying filaments that are best suited to specific needs. Given that filaments are plastics, polymer characterization techniques can be used to derive a lot of information about the materials being printed.

FFF is a thermally driven process. Therefore, thermal analysis techniques are particularly valuable for screening for processability.

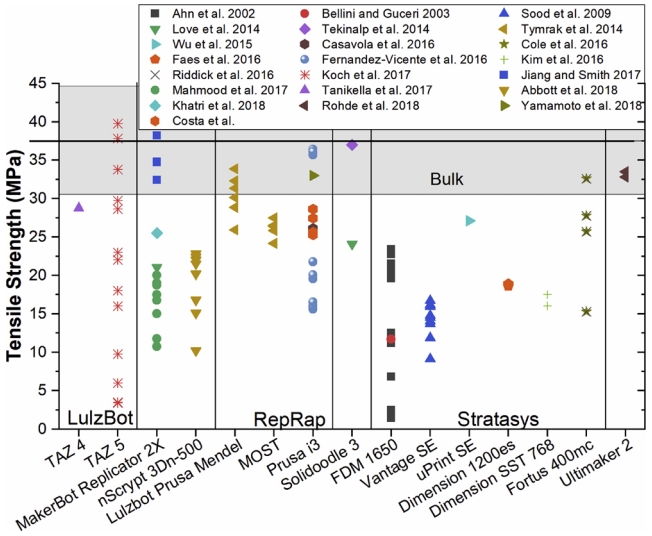

Fig. 6. Literature tensile strengths for x-oriented FFF-printed structures by printer. Each point represents the average of a print condition reported in the literature.

Thermogravimetric analysis (TGA) provides degradation onset temperatures, which are an important consideration for extrusion temperature. DSC can give T_g, T_c, and melt temperature (T_m), which represent lower bounds for T_{ext} and upper temperatures for T_{bed} in many cases.

Since FFF is achieved through extrusion of a molten polymer, the rheology of printed materials is an important consideration. Rotational rheology is the most common form in polymer research and can be used to determine temperature- and shear rate-dependent viscosity, as well as provide the data necessary for construction of a master curve for WLF analysis [112,139]. However, rotational rheology cannot achieve the full range of shear rates experienced in extrusion/FFF [112]. Although capillary rheology can only measure steady-shear phenomena, it can achieve the full range of shear rates experienced in FFF and provides the most process-relevant viscosity measurements [102].

Dynamic mechanical analysis (DMA), a popular technique for measuring the thermomechanical properties of polymer composites, can be used to characterize the viscoelastic behavior of the solid filaments. DMA is 10–100 times more sensitive to changes occurring at the glass transition than DSC. Multi-frequency DMA can provide the data necessary for master curve construction [17,140,141]. Additionally, DMA can be used to evaluate the presence of secondary phases and effectiveness of reinforcements [142–145].

6. Conclusions

ABS is the most commonly printed material, and we are capable of printing structures with mechanical properties that approximately match those of bulk ABS. However, given the wide range of printers and sources of ABS that are now on the market, it is not currently possible to know *a priori* how to achieve bulk performance with a given printer and ABS filament. ABS is a complex material, consisting of SAN and lightly cross-linked rubber particles that are grafted with SAN to improve dispersion. Additionally, ABS formulations often include additives to improve flow during processing, pigments to add color, and anitoxidants/UV absorbers to prevent degradation and maintain vibrant colors. It should be stressed that, while this review examines ABS performance, similar variability should be expected in any engineered plastic or composite used in FFF systems.

This review has focused on materials and processing considerations; however, printer selection also affected performance of FFF structures. This is because different printers contain different hardware and control systems with different set points and proportionality constants. Additionally, different printers operate using software packages that interpret gcode according to different rules/algorithms. Each print software will generate different gcodes based on their default settings, some of which cannot be altered.

Combined, this makes extracting fundamental insights on FFF

Table 2
Summary of processing parameters that lead to near-bulk tensile strength, sorted by ABS source.

ABS Source	Tensile Strength (MPa)	T_{ext} (°C)	T_{bed} (°C)	v_{print} (mm/s)	Layer Thickness (mm)	Raster Orientation (°)	Infill (%)	Ref.
3DXTECH	32.4	230	110	105	0.2	90	100	[127]
	34.7					45/-45		
	34.8					45		
	38.2					0		
ABS Nature	35.7	230	110	–	0.3	–	100	[121]
	36.1					–		
	36.4					45/-45		
ABS-M30	32.6	204	–	–	0.127	0	–	[124]
Filabot	33	230	80	60	0.2	45	100	[135]
GP35-ABS-NT	37	205	85	–	0.2	–	–	[115]
Maker Geeks	40.1	–	–	–	–	45/-45	–	[134]
	40.5					0/90		
MatterHackers	33.8	250	110	33.3	0.2	45/-45	95-97	[5]
	37.8					0	96	
	39.8					0	99	
Polylac® PA-747	30.5	245	110	60	0.2	90	100	[66]
	30.5	235						
	30.9	240						
Sinkral PD L 322	38	230	60	40	0.2	–	100	[137]
Taitalac 5000s	34.5	250	100	–	0.2	45	100	[132]
	39					0		

incredibly challenging. Informatics-based solutions that include multivariate statistical analysis techniques are likely to be key to understanding the physics of FFF. Sharing of detailed methods, including STL and gcode files, material information, and printer used as part of publications will aid the community in broadly advancing the performance and reliability of FFF structures.

References

[1] Y. Yang, Y. Chen, Y. Wei, Y. Li, 3D printing of shape memory polymer for functional part fabrication, Int. J. Adv. Manuf. Technol. 84 (2016) 2079–2095, https://doi.org/10.1007/s00170-015-7843-2.

[2] T.J. Coogan, D.O. Kazmer, Healing simulation for bond strength prediction of FDM, Rapid Prototyp. J. 23 (2017) 551–561, https://doi.org/10.1108/RPJ-03-2016-0051.

[3] V. Vega, J. Clements, T. Lam, A. Abad, B. Fritz, N. Ula, O.S. Es-Said, The effect of layer orientation on the mechanical properties and microstructure of a polymer, J. Mater. Eng. Perform. 20 (2011) 978–988, https://doi.org/10.1007/s11665-010-9740-z.

[4] A.A. D'Amico, A. Debaie, A.M. Peterson, Effect of layer thickness on irreversible thermal expansion and interlayer strength in fused deposition modeling, Rapid Prototyp. J. 23 (2017) 943–953, https://doi.org/10.1108/RPJ-05-2016-0077.

[5] C. Koch, L. Van Hulle, N. Rudolph, Investigation of mechanical anisotropy of the fused filament fabrication process via customized tool path generation, Addit. Manuf. 16 (2017) 138–145, https://doi.org/10.1016/j.addma.2017.06.003.

[6] C.S. Davis, K.E. Hillgartner, S.H. Han, J.E. Seppala, Mechanical strength of welding zones produced by polymer extrusion additive manufacturing, Addit. Manuf. 16 (2017) 162–166, https://doi.org/10.1016/j.addma.2017.06.006.

[7] Q. Sun, G.M. Rizvi, C.T. Bellehumeur, P. Gu, Effect of processing conditions on the bonding quality of FDM polymer filaments, Rapid Prototyp. J. 14 (2008) 72–80, https://doi.org/10.1108/13552540810862028.

[8] C. Yang, X. Tian, D. Li, Y. Cao, F. Zhao, C. Shi, Influence of thermal processing conditions in 3D printing on the crystallinity and mechanical properties of PEEK material, J. Mater. Process. Tech. 248 (2017) 1–7, https://doi.org/10.1016/j.jmatprotec.2017.04.027.

[9] K.C. Chuang, J.E. Grady, S.M. Arnold, R.D. Draper, E. Shin, C. Patterson, T. Santelle, C. Lao, M. Rhein, J. Mehl, A Fully Nonmetallic Gas Turbine Engine Enabled by Additive Manufacturing Part II : Additive Manufacturing and Characterization of Polymer Composites, (2015).

[10] C.S. Lee, S.G. Kim, H.J. Kim, S.H. Ahn, Measurement of anisotropic compressive strength of rapid prototyping parts, J. Mater. Process. Technol. 187–188 (2007) 627–630, https://doi.org/10.1016/j.jmatprotec.2006.11.095.

[11] A.K. Sood, R.K. Ohdar, S.S. Mahapatra, Improving dimensional accuracy of Fused Deposition Modelling processed part using grey Taguchi method, Mater. Des. 30 (2009) 4243–4252, https://doi.org/10.1016/j.matdes.2009.04.030.

[12] K. Thrimurthulu, P.M. Pandey, N.V. Reddy, Optimum part deposition orientation in fused deposition modeling, Int. J. Mach. Tools Manuf. 44 (2004) 585–594, https://doi.org/10.1016/j.ijmachtools.2003.12.004.

[13] L. Li, Q. Sun, C. Bellehumeur, P. Gu, Composite modeling and analysis for fabrication of FDM prototypes with locally controlled properties, J. Manuf. Process. 4 (2002) 129–141, https://doi.org/10.1016/S1526-6125(02)70139-4.

[14] T.A. Osswald, J. Puentes, J. Kattinger, Fused filament fabrication melting model, Addit. Manuf. 22 (2018) 51–59, https://doi.org/10.1016/j.addma.2018.04.030.

[15] Y. Zhang, Y. Chou, Three-dimensional finite element analysis simulations of the fused deposition modelling process, Proc. Inst. Mech. Eng. Part B J. Eng. Manuf. 220 (2006) 1663–1671, https://doi.org/10.1243/09544054JEM572.

[16] X. Zhou, S. Hsieh, Y. Sun, Experimental and numerical investigation of the thermal behaviour of polylactic acid during the fused deposition process, Virtual Phys. Prototyp. 12 (2017) 221–233, https://doi.org/10.1080/17452759.2017.1317214.

[17] A. D'Amico, A.M. Peterson, An adaptable FEA simulation of material extrusion additive manufacturing heat transfer in 3D, Addit. Manuf. 21 (2018) 422–430, https://doi.org/10.1016/j.addma.2018.02.021.

[18] Y. Zhang, V. Shapiro, Linear-time thermal simulation of as-manufactured fused deposition modeling components, J. Manuf. Sci. Eng. 140 (2018) 1–11.

[19] A. Kantaros, D. Karalekas, Fiber Bragg grating based investigation of residual strains in ABS parts fabricated by fused deposition modeling process, Mater. Des. 50 (2013) 44–50, https://doi.org/10.1016/j.matdes.2013.02.067.

[20] W. Wu, P. Geng, G. Li, D. Zhao, H. Zhang, J. Zhao, Influence of layer thickness and raster angle on the mechanical properties of 3D-Printed PEEK and a comparative mechanical study between PEEK and ABS, Materials 8 (2015) 5834–5846, https://doi.org/10.3390/ma8095271.

[21] S.H. Ahn, M. Montero, D. Odell, S. Roundy, P.K. Wright, Anisotropic material properties of fused deposition modeling ABS, Rapid Prototyp. J. 8 (2002) 248–257, https://doi.org/10.1108/13552540210441166.

[22] S. Ziemian, M. Okwara, C.W. Ziemian, Tensile and fatigue behavior of layered acrylonitrile butadiene styrene, Rapid Prototyp. J. 21 (2015) 270–278, https://doi.org/10.1108/RPJ-09-2013-0086.

[23] J.A. Brydson, Plastics Materials, 7th ed., Butterworth Heinemann, Boston, 1999.

[24] M. Kaveh, M. Badrossamay, E. Foroozmehr, A.H. Etefagh, Optimization of the printing parameters affecting dimensional accuracy and internal cavity for HIPS material used in fused deposition modeling processes, J. Mater. Process. Tech. 226 (2015) 280–286, https://doi.org/10.1016/j.jmatprotec.2015.07.012.

[25] N.G. Tanikella, B. Wittbrodt, J.M. Pearce, Tensile strength of commercial polymer materials for fused filament fabrication 3D printing, Addit. Manuf. 15 (2017) 40–47, https://doi.org/10.1016/j.addma.2017.03.005.

[26] H. Kadry, T.A. Al-hilal, A. Keshavarz, F. Alam, C. Xu, A. Joy, F. Ahsan, Multi-purposable filaments of HPMC for 3D printing of medications with tailored drug release and timed-absorption, Int. J. Pharm. 544 (2018) 285–296, https://doi.org/10.1016/j.ijpharm.2018.04.010.

[27] K.R. Hart, J.B. Frketic, J.R. Brown, Recycling meal-ready-to-eat (MRE) pouches into polymer fi lament for material extrusion additive manufacturing, Addit. Manuf. 21 (2018) 536–543, https://doi.org/10.1016/j.addma.2018.04.011.

[28] M. Domingo-Espin, J.M. Puigoriol-Forcada, A. Garcia-Granada, J. Llumà, S. Borros, G. Reyes, Mechanical property characterization and simulation of fused deposition modeling Polycarbonate parts, Mater. Des. 83 (2015) 670–677, https://doi.org/10.1016/j.matdes.2015.06.074.

[29] D. Roberson, C.M. Shemelya, E. Macdonald, R. Wicker, Expanding the applicability of FDM-type technologies through materials development, Rapid Prototyp. J. 21 (2015) 137–143, https://doi.org/10.1108/RPJ-12-2014-0165.

[30] O.S. Carneiro, A.F. Silva, R. Gomes, Fused deposition modeling with polypropylene, Mater. Des. 83 (2015) 768–776, https://doi.org/10.1016/j.matdes.2015.06.053.

[31] J.M. Puigoriol-Forcada, A. Alsina, A.G. Salazar-Martín, G. Gomez-Gras, M.A. Pérez, Flexural fatigue properties of polycarbonate fused-deposition modelling specimens, Mater. Des. 155 (2018) 414–421, https://doi.org/10.1016/j.matdes.2018.06.018.

[32] R. De Santis, A. Gloria, T. Russo, A. Ronca, U. D'Amora, D. Ronca, L. Ambrosio, Viscoelastic properties of rapid prototyped magnetic nanocomposite scaffolds for osteochondral tissue regeneration, Procedia CIRP 49 (2016) 76–82, https://doi.org/10.1016/j.procir.2015.07.037.

[33] M. Mohseni, D.W. Hutmacher, N.J. Castro, Independent evaluation of medical-grade bioresorbable filaments for fused deposition modelling/fused filament fabrication of tissue engineered constructs, Polymers 10 (2018) 40, https://doi.org/10.3390/polym10010040.

[34] J. Wang, H. Xie, Z. Weng, T. Senthil, L. Wu, A novel approach to improve mechanical properties of parts fabricated by fused deposition modeling, Mater. Des. 105 (2016) 152–159, https://doi.org/10.1016/j.matdes.2016.05.078.

[35] B. Valentan, Ž. Kadivnik, T. Brajlih, A. Anderson, I. Drstvenšek, Processing poly (ether etherketone) on a 3D printer for thermoplastic modelling, Mater. Technol. 47 (2013) 715–721.

[36] M. Vaezi, S. Yang, Extrusion-based additive manufacturing of PEEK for biomedical applications, Virtual Phys. Prototyp. 10 (2015) 123–135, https://doi.org/10.1080/17452759.2015.1097053.

[37] V. Kishore, X. Chen, C. Ajinjeru, A.A. Hassen, J. Lindahl, J. Failla, V. Kunc, C. Duty, Additive manufacturing of high performance semicrystalline thermoplastics and their composites, Proc. 27th Annu. Int. Solid Free. Fabr. Symp. (2016), pp. 906–915.

[38] S. Berretta, R. Davies, Y.T. Shyng, Y. Wang, O. Ghita, Fused deposition modelling of high temperature polymers: exploring CNT PEEK composites, Polym. Test. 63 (2017) 251–262, https://doi.org/10.1016/j.polymertesting.2017.08.024.

[39] M.F. Arif, S. Kumar, K.M. Varadarajan, W.J. Cantwell, Performance of biocompatible PEEK processed by fused deposition additive manufacturing, Mater. Des. 146 (2018) 249–259, https://doi.org/10.1016/j.matdes.2018.03.015.

[40] R.J. Zaldivar, D.B. Witkin, T. McLouth, D.N. Patel, K. Schmitt, J.P. Nokes, Influence of processing and orientation print effects on the mechanical and thermal behavior of 3D-Printed ULTEM 9085 Material, Addit. Manuf. 13 (2017) 71–80, https://doi.org/10.1016/j.addma.2016.11.007.

[41] G. Cicala, G. Ognibene, S. Portuesi, I. Blanco, M. Rapisarda, E. Pergolizzi, G. Recca, Comparison of ultem 9085 used in fused deposition modelling (FDM) with polytherimide blends, Materials 11 (2018) 285, https://doi.org/10.3390/ma11020285.

[42] N.E. Zander, M. Gillan, R.H. Lambeth, Recycled polyethylene terephthalate as a new FFF feedstock material, Addit. Manuf. 21 (2018) 174–182, https://doi.org/10.1016/j.addma.2018.03.007.

[43] B.M. Tymrak, M. Kreiger, J.M. Pearce, Mechanical properties of components fabricated with open-source 3-D printers under realistic environmental conditions, Mater. Des. 58 (2014) 242–246, https://doi.org/10.1016/j.matdes.2014.02.038.

[44] L. Wang, W.M. Gramlich, D.J. Gardner, Improving the impact strength of Poly (lactic acid) (PLA) in fused layer modeling (FLM), Polymer 114 (2017) 242–248, https://doi.org/10.1016/j.polymer.2017.03.011.

[45] J.M. Chacón, M.A. Caminero, E. García-Plaza, P.J. Núñez, Additive manufacturing of PLA structures using fused deposition modelling: effect of process parameters on mechanical properties and their optimal selection, Mater. Des. 124 (2017) 143–157, https://doi.org/10.1016/j.matdes.2017.03.065.

[46] P. Ravi, P.S. Shiakolas, T.R. Welch, Poly-l-lactic acid: pellets to fiber to fused filament fabricated scaffolds, and scaffold weight loss study, Addit. Manuf. 16 (2017) 167–176, https://doi.org/10.1016/j.addma.2017.06.002.

[47] F.A. Cruz Sanchez, H. Boudaoud, S. Hoppe, M. Camargo, Polymer recycling in an open-source additive manufacturing context: mechanical issues, Addit. Manuf. 17 (2017) 87–105, https://doi.org/10.1016/j.addma.2017.05.013.

[48] J.J. Laureto, J.M. Pearce, Anisotropic mechanical property variance between ASTM D638-14 type i and type iv fused filament fabricated specimens, Polym. Test. 68 (2018) 294–301, https://doi.org/10.1016/j.polymertesting.2018.04.029.

[49] W. Jo, O.-C. Kwon, M.-W. Moon, Investigation of influence of heat treatment on mechanical strength of FDM printed 3D objects, Rapid Prototyp. J. 24 (2018) 637–644, https://doi.org/10.1108/RPJ-06-2017-0131.

[50] F. Arbeiter, M. Spoerk, J. Wiener, A. Gosch, G. Pinter, Fracture mechanical characterization and lifetime estimation of near-homogeneous components produced by fused filament fabrication, Polym. Test. 66 (2018) 105–113, https://doi.

org/10.1016/j.polymertesting.2018.01.002.
[51] G. Cicala, D. Giordano, C. Tosto, A. Recca, I. Blanco, Polylactide (PLA) filaments a biobased solution for additive manufacturing: correlating rheology and thermomechanical properties with printing quality, Materials 11 (2018) 1191, https://doi.org/10.3390/ma11071191.
[52] M. Spoerk, J. Gonzalez-Gutierrez, J. Sapkota, S. Schuschnigg, C. Holzer, Effect of the printing bed temperature on the adhesion of parts produced by fused filament fabrication, Plast. Rubber Compos. 47 (2018) 17–24, https://doi.org/10.1080/14658011.2017.1399531.
[53] G. Gomez-Gras, R. Jerez-Mesa, J.A. Travieso-Rodriguez, J. Lluma-Fuentes, Fatigue performance of fused filament fabrication PLA specimens, Mater. Des. 140 (2018) 278–285, https://doi.org/10.1016/j.matdes.2017.11.072.
[54] G.W. Melenka, J.S. Schofield, M.R. Dawson, J.P. Carey, Evaluation of dimensional accuracy and material properties of the MakerBot 3D desktop printer, Rapid Prototyp. J. 21 (2015) 618–627, https://doi.org/10.1108/RPJ-09-2013-0093.
[55] H. Li, T. Wang, J. Sun, Z. Yu, The effect of process parameters in fused deposition modelling on bonding degree and mechanical properties, Rapid Prototyp. J. 24 (2018) 80–92, https://doi.org/10.1108/RPJ-06-2016-0090.
[56] V. Srinivas, C.S.J. van Hooy-Corstjens, J.A.W. Harings, Correlating molecular and crystallization dynamics to macroscopic fusion and thermodynamic stability in fused deposition modeling; a model study on polylactides, Polymer 142 (2018) 348–355, https://doi.org/10.1016/j.polymer.2018.03.063.
[57] V.E. Kuznetsov, A.N. Solonin, O.D. Urzhumtsev, R. Schilling, A.G. Tavitov, Strength of PLA components fabricated with fused deposition technology using a desktop 3D printer as a function of geometrical parameters of the process, Polymers 10 (2018) 313, https://doi.org/10.3390/polym10030313.
[58] B. Wittbrodt, J.M. Pearce, The effects of PLA color on material properties of 3-D printed components, Addit. Manuf. 8 (2015) 110–116, https://doi.org/10.1016/j.addma.2015.09.006.
[59] A. Tsouknidas, M. Pantazopoulos, I. Katsoulis, D. Fasnakis, S. Maropoulos, N. Michailidis, Impact absorption capacity of 3D-printed components fabricated by fused deposition modelling, Mater. Des. 102 (2016) 41–44, https://doi.org/10.1016/j.matdes.2016.03.154.
[60] Y. Song, Y. Li, W. Song, K. Yee, K.-Y. Lee, V.L. Tagarielli, Measurements of the mechanical response of unidirectional 3D-printed PLA, Mater. Des. 123 (2017) 154–164, https://doi.org/10.1016/j.matdes.2017.03.051.
[61] A.M. Baker, J. McCoy, B.S. Majumdar, B. Rumley-Ouellette, J. Wahry, A.N. Marchi, J.D. Bernadin, D. Spernjak, Measurement and modelling of thermal and mechanical anisotropy of parts additively manufactured using fused deposition modelling (FDM), in: F.-K. Chang, F. Kopsaftopoulos (Eds.), Struct. Heal. Monit, 2017, https://doi.org/10.12783/shm2017/13917.
[62] R.T.L. Ferreira, I.C. Amatte, T.A. Dutra, D. Bürger, Experimental characterization and micrography of 3D printed PLA and PLA reinforced with short carbon fibers, Compos. Part B 124 (2017) 88–100, https://doi.org/10.1016/j.compositesb.2017.05.013.
[63] S.O. Akande, K. Dalgarno, J. Munguia, Process control testing for fused filament fabrication, Rapid Prototyp. J. 23 (2017) 246–256, https://doi.org/10.1108/RPJ-07-2015-0084.
[64] M. Spoerk, F. Arbeiter, H. Cajner, J. Sapkota, C. Holzer, Parametric optimization of intra- and inter-layer strengths in parts produced by extrusion-based additive manufacturing of poly(lactic acid), J. Appl. Polym. Sci. 134 (2017) 45401, https://doi.org/10.1002/app.45401.
[65] W.S. Yerazunis, J.C. Barnwell III, D.N. Nikovski, Strengthening ABS, nylon, and polyester 3D printed parts by stress tensor aligned deposition paths and five-axis printing, Solid Free. Fabr. Proc. (2016).
[66] H. Li, S. Zhang, Z. Yi, J. Li, A. Sun, J. Guo, G. Xu, Bonding quality and fracture analysis of polyamide 12 parts fabricated by fused deposition modeling, Rapid Prototyp. J. 23 (2017) 973–982, https://doi.org/10.1108/RPJ-03-2016-0033.
[67] A.N. Dickson, J.N. Barry, K.A. McDonnell, D.P. Dowling, Fabrication of continuous carbon, glass and Kevlar fibre reinforced polymer composites using additive manufacturing, Addit. Manuf. 16 (2017) 146–152, https://doi.org/10.1016/j.addma.2017.06.004.
[68] G. Ellson, X. Carrier, J. Walton, S.F. Mahmood, K. Yang, J. Salazar, W.E. Voit, Tough thiourethane thermoplastics for fused filament fabrication, J. Appl. Polym. Sci. 135 (2018) 45574, https://doi.org/10.1002/app.45574.
[69] L. Wang, D.J. Gardner, Effect of fused layer modeling (FLM) processing parameters on impact strength of cellular polypropylene, Polymer. 113 (2017) 74–80, https://doi.org/10.1016/j.polymer.2017.02.055.
[70] E. Fuenmayor, M. Forde, A.V. Healy, D.M. Devine, J.G. Lyons, C. McConville, I. Major, Material considerations for fused-filament fabrication of solid dosage forms, Pharmaceutics. 10 (2018) 44, https://doi.org/10.3390/pharmaceutics10020044.
[71] J.M. Nasereddin, N. Wellner, M. Alhijjaj, P. Belton, S. Qi, Development of a simple mechanical screening method for predicting the feedability of a pharmaceutical FDM 3D printing filament, Pharm. Res. 35 (2018) 151.
[72] G. Kollamaram, D.M. Croker, G.M. Walker, A. Goyanes, A.W. Basit, S. Gaisford, Low temperature fused deposition modeling (FDM) 3D printing of thermolabile drugs, Int. J. Pharm. 545 (2018) 144–152, https://doi.org/10.1016/j.ijpharm.2018.04.055.
[73] C.R. Rocha, A.R. Torrado Perez, D.A. Roberson, C.M. Shemelya, E. Macdonald, R.B. Wicker, Novel ABS-based binary and ternary polymer blends for material extrusion 3D printing, J. Mater. Res. 29 (2014) 1859–1866, https://doi.org/10.1557/jmr.2014.158.
[74] A.R. Torrado, C.M. Shemelya, J.D. English, Y. Lin, R.B. Wicker, D.A. Roberson, Characterizing the effect of additives to ABS on the mechanical property anisotropy of specimens fabricated by material extrusion 3D printing, Addit. Manuf. 6 (2015) 16–29, https://doi.org/10.1016/j.addma.2015.02.001.
[75] P.M. Toal Jr, L.J. Holmes, R.X. Rodriguez, E.D. Wetzel, Microstructured monofilament via thermal drawing of additively manufactured preforms, Addit. Manuf. 16 (2017) 12–23, https://doi.org/10.1016/j.addma.2017.03.009.
[76] ASM International, Characterization and Failure Analysis of Plastics, ASM International, (2003).
[77] T. D'Amico, C. Barrett, J. Presing, A.M. Peterson, Micromechanical Modeling of Irreversible Thermal Strain, Addit. Manuf 27 (2019) 91–98, https://doi.org/10.1016/j.addma.2019.02.019.
[78] C. Kousiatza, D. Karalekas, In-situ monitoring of strain and temperature distributions during fused deposition modeling process, Mater. Des. 97 (2016) 400–406, https://doi.org/10.1016/j.matdes.2016.02.099.
[79] J.E. Seppala, K.D. Migler, Infrared thermography of welding zones produced by polymer extrusion additive manufacturing, Addit. Manuf. 12 (2016) 71–76, https://doi.org/10.1016/j.addma.2016.06.007.
[80] R.B. Dinwiddie, V. Kunc, J.M. Lindal, B. Post, R.J. Smith, L. Love, C.E. Duty, Infrared imaging of the polymer 3D-printing process, Proc. SPIE (2014) 910502, , https://doi.org/10.1117/12.2053425.
[81] C. Bellehumeur, L. Li, Q. Sun, P. Gu, Modeling of bond formation between polymer filaments in the fused deposition modeling process, J. Manuf. Process. 6 (2004) 170–178, https://doi.org/10.1016/S1526-6125(04)70071-7.
[82] J.P. Thomas, J.F. Rodriguez, Modeling the fracture strength between fused-deposition extruded roads, Solid Free. Fabr. Proc. (2000) 17–23.
[83] S.F. Costa, F.M. Duarte, J.A. Covas, Thermal conditions affecting heat transfer in FDM/FFE: a contribution towards the numerical modelling of the process, Virtual Phys. Prototyp. 10 (2015) 35–46, https://doi.org/10.1080/17452759.2014.984042.
[84] Y. Zhou, T. Nyberg, G. Xiong, D. Liu, Temperature analysis in the fused deposition modeling process, 2016 3rd Int. Conf. Inf. Sci. Control Eng. (2016) 678–682, https://doi.org/10.1109/ICISCE.2016.150.
[85] X. Zhou, S. Hsieh, Thermal analysis of fused deposition modeling process using infrared thermography imaging and finite element modeling, Proc. SPIE (2017) 1021409, , https://doi.org/10.1117/12.2262796.
[86] S.F. Costa, F.M. Duarte, J.A. Covas, Estimation of filament temperature and adhesion development in fused deposition techniques, J. Mater. Process. Technol. 245 (2017) 167–179, https://doi.org/10.1016/j.jmatprotec.2017.02.026.
[87] J. Zhang, X.Z. Wang, W.W. Yu, Y.H. Deng, Numerical investigation of the influence of process conditions on the temperature variation in fused deposition modeling, Mater. Des. 130 (2017) 59–68, https://doi.org/10.1016/j.matdes.2017.05.040.
[88] C. McIlroy, P.D. Olmsted, Disentanglement effects on welding behaviour of polymer melts during the fused-filament-fabrication method for additive manufacturing, Polymer 123 (2017) 376–391.
[89] Y.H. Kim, R.P. Wool, A theory of healing at a polymer-polymer interface, Macromolecules 16 (1983) 1115–1120, https://doi.org/10.1021/ma00241a013.
[90] R.P. Wool, K.M. O'Connor, A theory of crack healing in polymers, J. Appl. Phys. 52 (1981) 5953–5963.
[91] C. McIlroy, P.D. Olmsted, Deformation of an amorphous polymer during the fused-filament-Fabrication method for additive manufacturing, J. Rheol. 61 (2017) 379.
[92] D.P. Cole, J.C. Riddick, H.M.I. Jaim, K.E. Strawhecker, N.E. Zander, Interfacial mechanical behavior of 3D printed ABS, J. Appl. Polym. Sci. 133 (2016) 43671, https://doi.org/10.1002/app.43671.
[93] N.V. Pogodina, V.P. Lavrenko, S. Srinivas, H.H. Winter, Rheology and structure of isotactic polypropylene near the gel point: quiescent and shear-induced crystallization, Polymer 42 (2001) 9031–9043, https://doi.org/10.1016/S0032-3861(01)00402-5.
[94] Y. Lee, R.S. Porter, Effects of Thermal History on Crystallization of Poly(ether ether ketone) (PEEK), Macromolecules 2776 (1988) 2770–2776.
[95] A. Alizadeh, S. Sohn, J. Quinn, H. Marand, L.C. Shank, H. Darrell Iler, Influence of structural and topological constraints on the crystallization and melting behavior of polymers: 3. Bisphenol A polycarbonate, Macromolecules. 34 (2001) 4066–34078, https://doi.org/10.1021/ma001417s.
[96] O.O. Mykhaylyk, P. Chambon, C. Impradice, J.P.A. Fairclough, N.J. Terrill, A.J. Ryan, Control of structural morphology in shear-induced crystallization of polymers, Macromolecules 43 (2010) 2389–2405, https://doi.org/10.1021/ma902495z.
[97] B.P. Heller, D.E. Smith, D.A. Jack, Effects of extrudate swell and nozzle geometry on fiber orientation in Fused Filament Fabrication nozzle flow, Addit. Manuf. 12 (2016) 252–264, https://doi.org/10.1016/j.addma.2016.06.005.
[98] P.P. Parlevliet, H.E.N. Bersee, A. Beukers, Residual stresses in thermoplastic composites - a study of the literature. Part III: effects of thermal residual stresses, Compos. Part A Appl. Sci. Manuf. 38 (2007) 1581–1596, https://doi.org/10.1016/j.compositesa.2006.12.005.
[99] K. Prashantha, M.F. Lacrampe, P. Krawczak, Processing and characterization of halloysite nanotubes filled polypropylene nanocomposites based on a masterbatch route: effect of halloysites treatment on structural and mechanical properties, Express Polym. Lett. 5 (2011) 295–307, https://doi.org/10.3144/expresspolymlett.2011.30.
[100] E. Fischer, H. Sterzel, G. Wegner, Investigation of the structure of solution grown crystals of lactide copolymers by means of chemical reactions, Kolloid-Zeitschrift Und Zeitschrift Für Polym. 251 (1973) 980.
[101] M.L. Williams, R.F. Landel, J.D. Ferry, The temperature dependence of relaxation mechanisms in amorphous polymers and other glass-forming liquids, J. Am. Chem. Soc. 77 (1955) 3701–3707.
[102] T. Osswald, N. Rudolph, Polymer rheology, in: T. Osswald, N.B.T.-P.R. Rudolph (Eds.), Hanser, 2015, pp. I–XI, , https://doi.org/10.3139/9781569905234.fm.

[103] K.A. Welp, R.P. Wool, S.K. Satija, S. Pispas, J. Mays, Dynamics of polymer interdiffusion: the ripple experiment, Macromolecules 31 (1998) 4915–4925, https://doi.org/10.1021/ma971692n.
[104] K. Jud, H.H. Kausch, J.G. Williams, Fracture mechanics studies of crack healing and welding of polymers, J. Mater. Sci. 16 (1981) 204–210, https://doi.org/10.1007/BF00552073.
[105] S.R. White, N.R. Sottos, P.H. Geubelle, J.S. Moore, M.R. Kessler, S.R. Sriram, E.N. Brown, S. Viswanathan, Autonomic healing of polymer composites, Nature 409 (2001) 794–797, https://doi.org/10.1038/35057232.
[106] R.P. Wool, Self-healing materials: a review, Soft Matter 4 (2008) 400–418, https://doi.org/10.1039/b711716g.
[107] M.A.M. Rahmathullah, G.R. Palmese, Crack-healing behavior of epoxy-amine thermosets, J. Appl. Polym. Sci. 113 (2009) 2191–2201.
[108] A.M. Peterson, H. Kotthapalli, M.A.M. Rahmathullah, G.R. Palmese, Investigation of interpenetrating polymer networks for self-healing applications, Compos. Sci. Technol. 72 (2012) 330–336, https://doi.org/10.1016/j.compscitech.2011.11.022.
[109] B.J. Blaiszik, S.L.B. Kramer, S.C. Olugebefola, J.S. Moore, N.R. Sottos, S.R. White, Self-healing polymers and composites, Annu. Rev. Mater. Sci. 40 (2010) 19.1-19.33.
[110] S. Prager, M. Tirrell, The healing process at polymer-polymer interfaces, J. Chem. Phys. 75 (1981) 5194–5198, https://doi.org/10.1063/1.441871.
[111] P.-G. DeGennes, Interpenetration of polymers at an interface, C. R. Seances Acad. Sci, Ser. B. 291 (1980) 219–221.
[112] J.E. Seppala, S.H. Han, K.E. Hillgartner, C.S. Davis, K.B. Migler, Weld formation during material extrusion additive manufacturing, Soft Matter 13 (2017) 6761–6769, https://doi.org/10.1039/c7sm00950j.
[113] A. Bellini, S. Güçeri, Mechanical characterization of parts fabricated using fused deposition modeling, Rapid Prototyp. J. 9 (2003) 252–264, https://doi.org/10.1108/13552540310489631.
[114] L.J. Love, V. Kunc, O. Rios, C.E. Duty, A.M. Elliott, B.K. Post, R.J. Smith, C.A. Blue, The importance of carbon fiber to polymer additive manufacturing, J. Mater. Res. 29 (2014) 1893–1898, https://doi.org/10.1557/jmr.2014.212.
[115] H.L. Tekinalp, V. Kunc, G.M. Velez-garcia, C.E. Duty, L.J. Love, A.K. Naskar, C.A. Blue, S. Ozcan, Highly oriented carbon fiber – polymer composites via additive manufacturing, Compos. Sci. Technol. 105 (2014) 144–150, https://doi.org/10.1016/j.compscitech.2014.10.009.
[116] S. Hwang, E.I. Reyes, K. Moon, R.C. Rumpf, N.S. Kim, Thermo-mechanical characterization of metal/polymer composite filaments and printing parameter study for fused deposition modeling in the 3D printing process, J. Electron. Mater. 44 (2015) 771–777, https://doi.org/10.1007/s11664-014-3425-6.
[117] F. Ning, W. Cong, J. Qiu, J. Wei, S. Wang, Additive manufacturing of carbon fiber reinforced thermoplastic composites using fused deposition modeling, Compos. Part B 80 (2015) 369–378, https://doi.org/10.1016/j.compositesb.2015.06.013.
[118] C. Casavola, A. Cazzato, V. Moramarco, C. Pappalettere, Orthotropic mechanical properties of fused deposition modelling parts described by classical laminate theory, Mater. Des. 90 (2016) 453–458, https://doi.org/10.1016/j.matdes.2015.11.009.
[119] J. Du, Z. Wei, X. Wang, J. Wang, Z. Chen, An improved fused deposition modeling process for forming large-size thin-walled parts, J. Mater. Process. Technol. 234 (2016) 332–341, https://doi.org/10.1016/j.jmatprotec.2016.04.005.
[120] M. Faes, E. Ferraris, D. Moens, Influence of inter-layer cooling time on the quasi-static properties of ABS components produced via fused deposition modelling, Procedia CIRP (2016) 748–753, https://doi.org/10.1016/j.procir.2016.02.313.
[121] M. Fernandez-Vicente, W. Calle, S. Ferrandiz, A. Conejero, Effect of infill parameters on tensile mechanical behavior in desktop 3D printing, 3D print, Addit. Manuf. 3 (2016) 183–192, https://doi.org/10.1089/3dp.2015.0036.
[122] V. Francis, P.K. Jain, Experimental investigations on fused deposition modelling of polymer-layered silicate nanocomposite, Virtual Phys. Prototyp. 11 (2016) 109–121, https://doi.org/10.1080/17452759.2016.1172431.
[123] E. Kim, Y.-J. Shing, S.-H. Ahn, The effects of moisture and temperature on the mechanical properties of additive manufacturing components: fused deposition modeling, Rapid Prototyp. J. 22 (2016) 887–894, https://doi.org/10.1108/RPJ-08-2015-0095.
[124] J.C. Riddick, M.A. Haile, R. Von Wahlde, D.P. Cole, O. Bamiduro, T.E. Johnson, Fractographic analysis of tensile failure of acrylonitrile-butadiene-styrene fabricated by fused deposition modeling, Addit. Manuf. 11 (2016) 49–59, https://doi.org/10.1016/j.addma.2016.03.007.
[125] Z. Weng, J. Wang, T. Senthil, L. Wu, Mechanical and thermal properties of ABS/montmorillonite nanocomposites for fused deposition modeling 3D printing, Mater. Des. 102 (2016) 276–283, https://doi.org/10.1016/j.matdes.2016.04.045.
[126] T.J. Coogan, D.O. Kazmer, Bond and part strength in fused deposition modeling, Rapid Prototyp. J. 23 (2017) 414–422, https://doi.org/10.1108/RPJ-03-2016-0050.
[127] D. Jiang, D.E. Smith, Anisotropic mechanical properties of oriented carbon fiber filled polymer composites produced with fused filament fabrication, Addit. Manuf. 18 (2017) 84–94, https://doi.org/10.1016/j.addma.2017.08.006.
[128] S. Mahmood, A.J. Qureshi, K.L. Goh, D. Talamona, Tensile strength of partially filled FFF printed parts: experimental results, Rapid Prototyp. J. 23 (2017) 122–128, https://doi.org/10.1108/RPJ-10-2015-0151.
[129] C. Shemelya, A. De La Rosa, A.R. Torrado, K. Yu, J. Domanowski, P.J. Bonacuse, R.E. Martin, M. Juhasz, F. Hurwitz, R.B. Wicker, B. Conner, E. MacDonald, D.A. Roberson, Anisotropy of thermal conductivity in 3D printed polymer matrix composites for space based cube satellites, Addit. Manuf. 16 (2017) 186–196, https://doi.org/10.1016/j.addma.2017.05.012.
[130] A.C. Abbott, G.P. Tandon, R.L. Bradford, H. Koerner, J.W. Baur, Process-structure-property effects on ABS bond strength in fused filament fabrication, Addit. Manuf. 19 (2018) 29–38, https://doi.org/10.1016/j.addma.2017.11.002.
[131] B. Khatri, K. Lappe, M. Habedank, T. Mueller, C. Megnin, T. Hanemann, Fused deposition modeling of ABS-barium titanate composites: a simple route towards tailored dielectric devices, Polymers (Basel) 10 (2018) 666, https://doi.org/10.3390/polym10060666.
[132] M.A. Osman, M.R.A. Atia, Investigation of ABS-rice straw composite feedstock filament for FDM, Rapid Prototyp. J. 24 (2018) 1067–1075, https://doi.org/10.1108/RPJ-11-2017-0242.
[133] S. Rohde, J. Cantrell, A. Jerez, C. Kroese, D. Damiani, R. Gurnani, L. DiSandro, J. Anton, A. Young, D. Steinbach, P. Ifju, Experimental characterization of the shear properties of 3D–printed ABS and polycarbonate parts, Exp. Mech. 58 (2018) 871–884, https://doi.org/10.1007/s11340-017-0343-6.
[134] M.A. Ryder, D.A. Lados, G.S. Iannacchione, A.M. Peterson, Fabrication and properties of novel polymer-metal composites using fused deposition modeling, Compos. Sci. Technol. 158 (2018) 43–50, https://doi.org/10.1016/j.compscitech.2018.01.049.
[135] B.E. Yamamoto, A.Z. Trimble, B. Minei, M.N.G. Nejhad, Development of multi-functional nanocomposites with 3-D printing additive manufacturing and low graphene loading, J. Thermoplast. Compos. Mater. (2018) 1–26, https://doi.org/10.1177/0892705718759390.
[136] A.E. Costa, A. Ferreira, O.S. Carneiro, A study on extruded filament bonding in fused filament fabrication, Rapid Prototyp. J. (2018), https://doi.org/10.1108/RPJ-03-2018-0062.
[137] S. Dul, L. Fambri, A. Pegoretti, Fused deposition modelling with ABS–graphene nanocomposites, Compos. Part A 85 (2016) 181–191, https://doi.org/10.1016/j.compositesa.2016.03.013.
[138] M.H. Khaliq, R. Gomes, C. Fernandes, J. Nobrega, O.S. Carneiro, L.L. Ferras, On the use of high viscosity polymers in the fused filament fabrication process, Rapid Prototyp. J. 23 (2017) 727–735, https://doi.org/10.1108/RPJ-02-2016-0027.
[139] J. Bartolai, T.W. Simpson, R. Xie, Predicting strength of additively manufactured thermoplastic polymer parts produced using material extrusion, Rapid Prototyp. J. 24 (2018) 321–332, https://doi.org/10.1108/RPJ-02-2017-0026.
[140] M. Tajvidi, R.H. Falk, J.C. Hermanson, Time-temperature superposition principle applied to a kenaf-fiber/high- density polyethylene composite, J. Appl. Polym. Sci. 97 (2005) 1995–2004, https://doi.org/10.1002/app.21648.
[141] R.E. Jensen, G.R. Palmese, S.H. McKnight, Viscoelastic properties of alkoxy silane-epoxy interpenetrating networks, Int. J. Adhes. Adhes. 26 (2006) 103–115, https://doi.org/10.1016/j.ijadhadh.2005.03.004.
[142] G. Shi, M.Q. Zhang, M.Z. Rong, B. Wetzel, K. Friedrich, Friction and wear of low nanometer Si3N4 filled epoxy composites, Wear 254 (2003) 784–796, https://doi.org/10.1016/S0043-1648(03)00190-X.
[143] J. Jyoti, B.P. Singh, A.K. Arya, S.R. Dhakate, Dynamic mechanical properties of multiwall carbon nanotube reinforced ABS composites and their correlation with entanglement density, adhesion, reinforcement and C factor, RSC Adv. 6 (2016) 3997–4006, https://doi.org/10.1039/C5RA25561A.
[144] J. Lu, L.T. Drzal, Microfibrillated cellulose/cellulose acetate composites: effect of surface treatment, J. Polym. Sci. Part B: Polym. Phys. 48 (2010) 153–161.
[145] K.P. Menard, Dynamic Mechanical Analysis: A Practical Introduction, 2nd ed., Taylor & Francis, Boca Raton, FL, 2008.